Journal of Hydrology 603 (2021) 127171

Contents lists available at ScienceDirect

Journal of Hydrology

journal homepage: www.elsevier.com/locate/jhydrol

Research papers

Estimating soil water retention curves from soil thermal conductivity measurements

Yongwei Fu [a], Sen Lu [b], Tusheng Ren [c], Robert Horton [d], J.L. Heitman [a,*]

[a] Department of Crop & Soil Sciences, North Carolina State University, Raleigh 27695, United States
[b] Key Laboratory of Tree Breeding and Cultivation of State Forestry Administration, Chinese Academy of Forestry, Beijing 100091, China
[c] College of Land Science and Technology, China Agricultural University, Beijing 100091, China
[d] Department of Agronomy, Iowa State University, Ames 50011, United States

ARTICLE INFO

Keywords:
Thermal conductivity
Van Genuchten model
Water content
Soil water retention curve
Matric potential

ABSTRACT

The soil water retention curve represents the relationship between soil water content (θ) and matric potential (ψ). The van Genuchten (vG) model is commonly used to characterize the shape of a θ(ψ) curve. Based on the similarities between θ(ψ) curves and soil thermal conductivity (λ) versus θ curves, Lu and Dong proposed a unified conceptual λ(θ) model (LD model) for estimating λ(θ) curves from θ(ψ) curves. Their work makes it possible to relate the shapes of λ(θ) curves to θ(ψ) curves. In this study, we present an empirical approach to estimate the vG model parameter *m* from the LD model shape parameter *p* based on a model calibration with θ(ψ) and λ(θ) datasets obtained from 10 soils. The saturated water content θ_s and the vG model parameter α are estimated from selected soil properties (i.e., bulk density, particle density, particle size distribution and organic carbon content), and the residual water content θ_r is estimated from the LD model parameter θ_f. For model evaluation, the θ(ψ) curves of six soils were estimated from measured λ(θ) values and selected soil properties, and were compared to direct θ(ψ) measurements. The proposed method performed well with root mean square errors of estimated θ values ranging from 0.015 to 0.052 $cm^3\ cm^{-3}$ and bias ranging from −0.009 to 0.040 $cm^3\ cm^{-3}$. We conclude that the proposed method accurately estimates θ(ψ) curves from λ(θ) curves and selected soil properties.

1. Introduction

Describing and quantifying water and chemical storage and transport in the vadose zone requires knowledge of the soil water retention curve, which relates soil water matric potential (ψ) and water content (θ). The θ(ψ) curve is also a key soil property for estimating plant water availability, watershed runoff prediction, and environmental quality management (Bescansa et al., 2006; Miyata et al., 2007).

The θ(ψ) curves vary in space and time due to variations in soil properties, management, disturbance, and plant growth, among other factors. Consequently, θ(ψ) models have been developed to provide estimates when measurements are limited (Brooks and Corey, 1964; Campbell, 1974; van Genuchten, 1980; Fredlund and Xing, 1994; Kosugi, 1994; Dexter et al., 2008; Omuto, 2009). These models typically contain shape parameters, which can be obtained by fitting the θ(ψ) model to measured values. Unfortunately, collecting the data needed to estimate these model parameters can be time consuming. Several studies have been performed to estimate the parameters with pedo-transfer functions (Rawls and Brakensiek, 1985; Wösten et al., 2001; Weynants et al., 2009; Vereecken et al., 1989, 2010) and neural network analyses (Schaap and Bouten, 1996; Schaap and Leij, 1998; Merdun et al., 2006). However, the reliability of applying these relationships is uncertain and requires careful validation for regions or conditions beyond those under which they were originally developed.

Generally, there are four regimes (i.e., hydration, pendular, funicular, and capillary) defining the θ(ψ) curve along the path of increasing water content, which are dominated by two distinct principal forces: adsorption and capillarity (Tuller et al., 1999; Kim et al., 2015). The hydration regime refers to conditions where water molecules are adsorbed to mineral complexes by van der Waals attraction, cations and anions or hydrogen bonds of water (Lu and Likos, 2004). The pendular regime begins once discrete menisci are formed and individual water bridges are built near particle contacts (Mitarai and Nori, 2006). In the funicular regime, water bridges around the particles and water-filled

* Corresponding author.
E-mail address: jlheitman@ncsu.edu (J.L. Heitman).

https://doi.org/10.1016/j.jhydrol.2021.127171
Received 26 May 2021; Received in revised form 2 November 2021; Accepted 3 November 2021
Available online 10 November 2021

pores coexist. The capillary regime starts when the air phase occludes bubbles, and the pore-water instead of air occupies most of the voids. As θ increases, the energy level of pore water increases from hydration through the capillary regime, and each of the regimes modify soil thermal conductivity (λ) differently. Tarnawski and Gori (2002) divided the thermal conductivity-water content curve (λ(θ)) into four zones representing residual, transitory meniscus, micro/macro-pore capillary, and superfluous water. The range and boundary of each regime depends on the soil and liquid type and micro-structures (i.e., particle geometry, particle/pore size distribution, pore-water arrangement, and interfacial properties), which can be identified as the key governing factors for λ(θ) (Lipiec et al., 2007; Côté and Konrad, 2009). Interestingly, these factors can also be used to determine θ(ψ) curves. Based on the correlation between λ(θ) curves and θ(ψ) curves, McCumber and Pielke (1981) established an exponential equation to relate ψ and λ, and Reece (1996) developed a λ(ψ) relationship used to estimate ψ with a line heat dissipation sensor. Lu et al. (2019) presented a generalized λ(ψ) model for a selected ψ range ($\psi < -1000$ cm) and He et al. (2020) presented an improved λ(ψ) model covering the entire ψ range. Recently, Likos (2014) estimated λ(θ) from bimodal water retention curves using measurements of θ(ψ) curves for coarse-textured soils. Considering the similarities between the sigmoidal shapes of the θ(ψ) curve and the λ(θ)

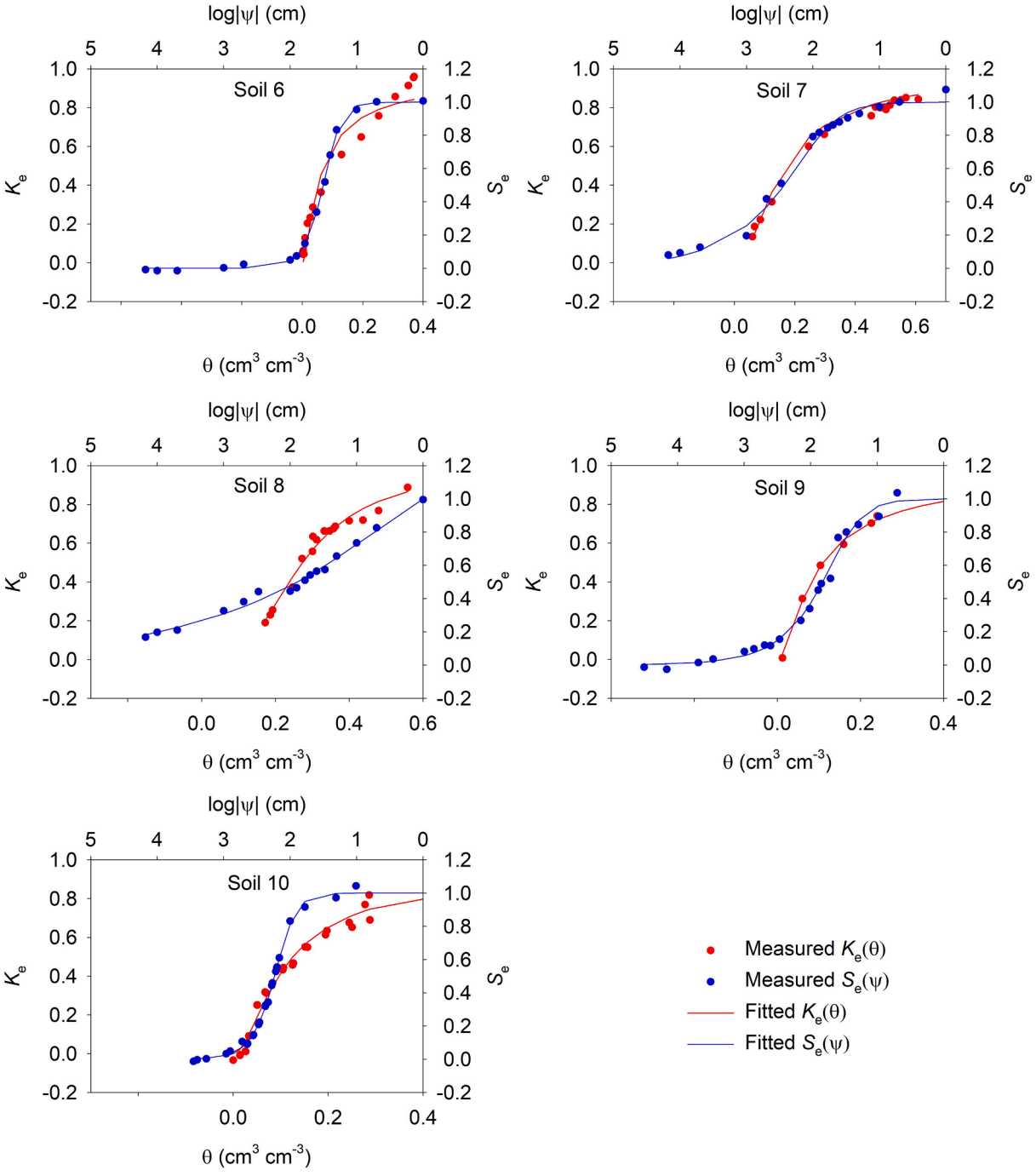

Fig. 1. Measured and fitted curves for the soil water retention curves (θ(ψ)) and thermal conductivity curves (λ(θ)) for Soils 6–10, where the θ(ψ) curves are expressed as S_e versus log|ψ| and λ(θ) curves are plotted as the normalized λ data (K_e) against θ. The red and blue circle points represent measured K_e(θ) and S_e(ψ) values, respectively. The red and blue solid lines indicate K_e(θ) and S_e(ψ) curves fitted by the LD model (Eqs. (2)–(4)) and the vG model (Eq. (1)), respectively. (For interpretation of the references to colour in this figure legend, the reader is referred to the web version of this article.)

curve, Lu and Dong (2015) proposed a closed form λ(θ) model like the van Genuchten (1980) (θ(ψ)) model. The model was fitted to λ(θ) measurements to determine model parameters. This work suggested that it might be possible to estimate θ(ψ) curves from λ(θ) curves. Such an approach has some advantages in that λ can be more easily measured than ψ over a range of conditions, particularly in the field (Ochsner and Baker, 2008).

The objective of this study is to develop a new approach to estimate van Genuchten (1980) (θ(ψ)) parameters from measured λ(θ) values and other easily measured soil properties. A new model is established based on measurements from 10 soils of varying texture and is evaluated with data representing another six soils.

2. Model development

2.1. The Lu and dong model

Numerous empirical parametric models have been proposed to describe the θ(ψ) curves. Among them, the van Genuchten (1980) model (vG model) has been used extensively,

$$S_e = \frac{\theta - \theta_r}{\theta_s - \theta_r} = \left[1 + (\alpha|\psi|)^{1/(1-m)}\right]^{-m} \quad (1)$$

where S_e is effective saturation, θ_s is the saturated water content (cm^3 cm^{-3}), θ_r is the residual water content (cm^3 cm^{-3}), α (<0, cm^{-1}) is related to the inverse of the air-entry pressure, and m ($0 < m < 1$) is a parameter related to pore-size distribution.

As illustrated in Fig. 1, both the θ(ψ) curves and λ(θ) curves have sigmoidal shapes. Based on observations and the characteristics of the sigmoid function, Lu and Dong (2015) proposed a closed-form equation analogous to the van Genuchten model to describe the λ(θ) curve,

$$K_e = \frac{\lambda - \lambda_{dry}}{\lambda_{sat} - \lambda_{dry}} = 1 - \left[1 + \left(\frac{\theta}{\theta_f}\right)^{1/(1-p)}\right]^{-p} \quad (2)$$

where K_e is the Kersten number, λ_{sat} and λ_{dry} are the thermal conductivity of saturated and dry soils (W m^{-1} K^{-1}), respectively, θ_f is the funicular water content which is the onset of the funicular regime (cm^3 cm^{-3}), and p ($0 < p < 1$) is defined as the pore fluid network connectivity parameter for λ(θ). Eq. (2) is hereafter denoted as the LD model.

The λ_{sat} and λ_{dry} values can be indirectly estimated from soil properties using empirical equations. For λ_{sat}, the following geometric mean equation has been widely used (Johansen, 1975),

$$\lambda_{sat} = \left(\lambda_q^q \lambda_o^{1-q}\right)^{1-\phi} \lambda_w^{\phi} \quad (3)$$

where q is the quartz content, λ_q, λ_o and λ_w are the thermal conductivities of quartz (7.7 W m^{-1} K^{-1}), other minerals (2.0 W m^{-1} K^{-1} for soils with q greater than 0.2, and 3.0 W m^{-1} K^{-1} for soils with $q \leq 0.2$) and water (0.594 W m^{-1} K^{-1} at 20 °C), respectively. In this study, we followed the assumption of Lu et al. (2007) that the quartz content (q) was equal to the sand content.

The parameter λ_{dry} can be estimated from an empirical linear relationship between λ_{dry} and ϕ (Lu et al., 2007):

$$\lambda_{dry} = -0.56\phi + 0.51 \quad (4)$$

Lu et al. (2007) reported that Eqs. (3) and (4) provided reliable estimates of λ_{sat} and λ_{dry}. When information about soil texture and porosity is not available, λ_{sat} and λ_{dry} are directly determined by fitting Eq. (2) to the available soil thermal conductivity versus water content (λ(θ)) data.

2.2. Estimating θ(ψ) curves from λ(θ) data

The four parameters θ_s, θ_r, α and m in the van Genuchten (1980) model can be determined by fitting Eq. (1) to θ versus ψ measurements. In this paper, we use the following approach to estimate these parameters from soil properties (organic carbon content, bulk density, particle density and soil texture) and λ(θ) measurements.

Commonly, θ_s is assumed to be equal to the soil porosity (ϕ):

$$\theta_s = \phi \quad (5)$$

There may exist an intrinsic relationship between a soil's θ(ψ) and the λ(θ) curves, such that a quantitative relationship between θ_f and θ_r is inherent. Lu and Dong (2015) proposed the following empirical relationship ($R^2 = 0.91$):

$$\theta_r = 0.54\theta_f \quad (6)$$

Based on measurements from undisturbed samples of 182 horizons of 40 soils, Weynants et al. (2009) applied global search algorithms and a one-step method to estimate the parameter α,

$$\alpha = exp(-4.3003 + 0.0138f_{sand} - 0.0097f_{clay} - 0.0992f_{OC}) \quad (7)$$

where f_{sand} is sand content (%, w/w), f_{clay} is clay content (%, w/w) and f_{OC} is soil organic carbon content (%, w/w). In this study, we converted the organic matter contents to f_{OC} values with a factor of 0.58, as soil organic matter contains approximately 58% carbon (Howard and Howard, 1990).

Considering the similarities between the shapes of θ(ψ) curves and λ(θ) curves, an empirical relationship between the VG model shape parameter m and the LD model shape parameter p was developed (details are shown in section 4.3).

2.3. Statistical analysis

In this study, we compared θ(ψ) data estimated from λ(θ) curves to directly measured θ(ψ) data. The estimated θ values at selected ψ values were evaluated using root mean square error (RMSE) and bias:

$$RMSE = \sqrt{\frac{\sum(\theta_{estimated} - \theta_{measured})^2}{N}} \quad (8)$$

$$Bias = \frac{\sum(\theta_{estimated} - \theta_{measured})}{N} \quad (9)$$

where N was the number of data pairs, and $\theta_{estimated}$ and $\theta_{measured}$ were the estimated and measured water content values, respectively.

3. Materials and methods

In this study, 16 soils were divided into calibration and validation groups based on two criteria: (1) the calibration group represented a variety of soil textures, which was a major factor controlling the θ(ψ) curves and λ(θ) curves; (2) the soils used in the validation group had available θ(ψ) and λ(θ) datasets and known soil properties (organic carbon content, bulk density, particle density and soil texture) because they were necessary for verification of the proposed approach. Thus, the θ(ψ) and λ(θ) datasets for 10 soils (Soils 1–10) representing a range of texture were used to calibrate and another six soils (Soils 11–16) were used to verify the proposed approach. For Soils 1–5, since their θ(ψ) and λ(θ) data were not available, we used the fitting parameters from Table 1 and Fig. 6a of Lu and Dong (2015). Tables 1 and 2 present the basic soil physical properties and the sources of the 16 soils.

For Soils 1–2 (Smits et al., 2010; Likos, 2014), an instrumented hanging column apparatus adapted from Smits et al. (2010) was used to make concurrent measurements of the θ(ψ) and λ(θ) curves. The θ values and corresponding λ values were measured with a soil water content sensor (ECH_2O EC-5, Decagon Devices, Pullman, WA) and a thermal property analyzer (SH-1, KD-2 Pro, Decagon Devices, Pullman, WA), respectively. The ψ values were measured with a tensiometer connected to a differential pressure transducer (Model P55D, Validyne Engineering

Table 1
Texture, particle size distribution, organic matter (OM) content, bulk density (ρ_b) and sources of soils (Soils 1–10) used for model calibration.

Soil no.	Texture	Particle size distribution			OM content	ρ_b	Sources
		Sand	Silt	Clay			
		%			%	g cm^{-3}	
1	sand	100	0	0	–	1.77	Smits et al. (2010)
2	sand	100	0	0	–	1.56	Likos (2014)
3	sand	100	0	0	–	1.67	Dong et al. (2015)
4	clay	0	0	100	–	1.31	Lu and Dong (2015)
5	clay	0	0	100	–	1.28	Lu and Dong (2015)
6	sand	100	0	0	–	1.67	Fu et al. (2021b)
7	silt loam	21	67	12	–	1.05	Fu et al. (2021b)
8	clay loam	24	49	27	–	1.20	Fu et al. (2021b)
9	sandy loam	67	21	12	0.86	1.41	Lu et al. (2008)
10	loam	40	49	11	0.49	1.30	Lu et al. (2008)

Table 2
Texture, particle size distribution, organic matter (OM) content, bulk density (ρ_b) and sources of soils (Soils 11–16) used for model validation.

Soil no.	Texture	Particle size distribution			OM content	ρ_b	Sources
		Sand	Silt	Clay			
		%			%	g cm^{-3}	
11	sand	93	1	6	0.07	1.60	Lu et al. (2008)
12	silt loam	27	51	22	1.19	1.34	Lu et al. (2008)
13	silty clay loam	19	54	27	0.39	1.29	Lu et al. (2008)
14	silt loam	11	70	19	0.84	1.33	Lu et al. (2008)
15	silty clay loam	8	60	32	3.02	1.32	Lu et al. (2008)
16	silt loam	2	73	25	4.40	1.20	Lu et al. (2008)

Corporation, Northridge, CA). The water content, thermal conductivity, and ψ sensors were installed in soil samples at the same horizontal plane so that ψ, λ and θ measurements could be made at selected matric potential and water content conditions.

Transient water desorption and water imbibition methods (TDIM), which have been used to obtain θ(ψ) curves for various types of soils (Wayllace and Lu, 2012), were used to determine the θ(ψ) curves of Soils 3–5 (Dong et al., 2015; Lu and Dong, 2015). Thermal sensors (SH-1, KD-2 Pro, Decagon Devices, Pullman, WA) were incorporated into the TDIM to facilitate concurrent measurements of both θ(ψ) and λ(θ) curves of Soils 3–5.

For Soils 6–8, the θ values at ψ of 0, −5, −10, −20, −30, −40, −50, −60, −80 and −100 cm were determined with a tension table (08.01 Sandbox, Eijkelkamp, Zeitz, Germany). Thermo-time domain reflectometry (Thermo-TDR) sensors were inserted vertically into the samples from the top to determine λ and θ. Details on thermo-TDR sensors were reported by Lu et al. (2017), and methods for determining λ and θ values from thermo-TDR sensor measurements were reported by Ren et al. (1999). The pressure plate extractor method was used to measure θ values at additional ψ values of −50, −100, −500, −1000 and −1500 kPa, and an additional measurement at 30 kPa was also included for Soil 10. To obtain λ and θ data corresponding to these conditions, a set of soil columns was prepared at θ values corresponding to selected ψ values based on the measured θ(ψ) data. Thermo-TDR sensors were used to measure λ and θ of each repacked soil column.

Soils 9–16, one from Iowa (Soil 10) and the others from China, were collected from the surface and subsurface layers, respectively (Lu et al., 2008). The soil samples were air dried, ground, and sieved through a 2-mm screen, and then packed as soil columns (50-mm inner diameter and 10-mm high) at desired bulk density (ρ_b) values. The pressure plate extractor method (Dane and Hopmans, 2002) was used to measure θ(ψ) curves for the $|\psi|$ range $\leq$ 1500 kPa. Thermo-TDR sensors were used to measure the λ and θ values for Soils 9–16.

4. Results and discussion

4.1. Similarities between θ(ψ) curves and λ(θ) curves

The measured θ(ψ) curves and λ(θ) curves for Soils 6–10 are presented in Fig. 1, where the θ(ψ) curves are expressed as S_e versus log$|\psi|$ (the common log of absolute ψ values in cm) and λ(θ) curves are plotted as the normalized λ data (K_e) against θ. The λ(θ) curves for these soils are generally sigmoidal in shape, which is in line with the reports of Lu and Dong (2015). In the residual water domain corresponding to large $|\psi|$ values (for $\theta < \theta_r$), soil water exists as thin films adsorbed to the soil particle surfaces (Tarnawski and Leong, 2000; Revil and Lu, 2013). The film thickness is so thin that heat conduction at this stage occurs mainly through the solid mineral phase, and λ is relatively constant over the range of these small θ values. This trait (flat segment of the λ(θ) curve) is smaller in coarse-textured soils (Soils 6 and 9). The larger the clay content of a soil, the more pronounced is the flat tail of the λ(θ) curve at small θ values. As $|\psi|$ decreases or θ increases (between θ_r and θ_f), water menisci form near the particle contacts, the surfaces of soil particles are coated gradually, and water bridges are formed between solid particles (Ewing and Horton, 2007). This significantly expands the heat transfer paths through the water bridges connecting particles and results in a rapidly increasing trend in λ with θ. At the inflection point θ_f, the menisci are fully interconnected to each other. The θ_f value is related to clay content: Fine-textured soils (e.g., Soils 7, 8 and 10) have larger θ_f values than coarse-textured soils (e.g., Soils 6 and 9). As θ becomes larger than θ_f, $|\psi|$ continues to decrease and the retained water enters the funicular regime where water bridges grow and begin to merge with adjacent ones to form a thick connected water-film around the soil particles. This results in further enhancement of λ, but the rate of change in λ with respect to θ gradually decreases. Eventually, $|\psi|$ becomes small as θ is close to saturation, and λ approaches its maximum value (λ_{sat}). Within this portion of the water retention regime, little change is observed in the λ values because further replacement of air with water does not have a large impact on the conductive heat transfer pathway.

Table 3
The root mean square error (RMSE), bias and coefficient of determination (R^2) between the fitted LD model (Eqs. (2)–(4)) values and the measured thermal conductivity values for Soils 6–10 in this study.

Soil no.	Texture	RMSE	Bias	R^2
		W m^{-1} K^{-1}	W m^{-1} K^{-1}	
6	sand	0.203	−0.065	0.96
7	silt loam	0.034	0.021	0.99
8	clay loam	0.038	0.003	0.97
9	sandy loam	0.023	0.005	1.00
10	loam	0.055	0.012	0.98
Average		**0.038**	**−0.005**	**0.97**

4.2. Performance of the LD model

We first used Eqs. (3) and (4) to estimate the λ_{sat} and λ_{dry}, respectively then Eq. (2) was fitted to measured data from Soils 6–10 in order to determine p values for a range of soil textures (with available $\lambda(\theta)$ and $\theta(\psi)$ datasets). As evident in Fig. 1, the fitted curves of the LD model capture the flat tail of the $\lambda(\theta)$ curve and the drastic onset of the pendular regime, as indicated by the rapid λ increases with θ increases. The slopes of the regression curves and the coefficients of determination (R^2) for all soils were greater than 0.96, indicating that the LD model fitted the measured values well (Table 3). Error analysis showed that the RMSE was within 0.023–0.203 W m^{-1} K^{-1} (with an average of 0.038 W m^{-1} K^{-1}), and the bias ranged from −0.065 to 0.021 W m^{-1} K^{-1} (with a mean of −0.005 W m^{-1} K^{-1}). Additionally, experimental results in Lu and Dong (2015) showed that for Soil 1–5, compared to the measured data, the fitted results by LD model had an average R^2 of 0.96 and an average RMSE of 0.133 W m^{-1} K^{-1}. Thus, the LD model provided reasonable fits to the measured values.

The pore fluid conductivity parameter, p, ranged from 0.41 to 0.69 on Soils 1–10 (Table 4). Lu and Dong (2015) obtained a similar range, 0.41 to 0.79, for 27 soils that covered a wide range of textures. This was no coincidence because p reflected the rate of change in λ with θ. The influence of parameter p on the shape of the $\lambda(\theta)$ curve is illustrated in Fig. 2, where λ_{dry}, λ_{sat} and θ_f are set at 0.3 W m^{-1} K^{-1}, 2.0 W m^{-1} K^{-1} and 0.05 cm^3 cm^{-3}, respectively, and p ranges from 0.3 to 0.9. With increasing p values, the sensitivity of λ to the change in θ increased at large θ values, and the $\lambda(\theta)$ curves had more pronounced "flat tails" at low θ values. However, the larger the soil clay content, the more pronounced the flat tail of the $\lambda(\theta)$ curve at small θ values and the more gradual the λ response to θ increases. Most soils had moderate p values ($0.4 < p < 0.8$) rather than extreme values.

4.3. Estimating $\theta(\psi)$ curves from $\lambda(\theta)$ measurements

By fitting Eq. (1) to $\theta(\psi)$ measurements and fitting Eqs. (2)–(4) to measured thermal conductivity data, we obtained the vG model parameters (θ_s, θ_r, α, m) and the LD model parameters (λ_{sat}, λ_{dry}, θ_f, p) of Soils 6–10. All of the parameters for Soils 1–5 are from Table 1 and Fig. 6a of Lu and Dong (2015). We further examined the paired m and p values of the 10 soils that represented a wide range of soil texture (e.g.,

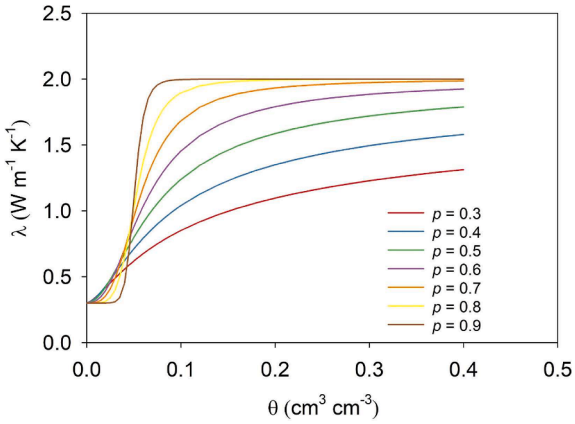

Fig. 2. The influence of parameter p on thermal conductivity curves ($\lambda(\theta)$) obtained with Eqs. (2)-(4). λ_{dry}, λ_{sat} and θ_f values are set at 0.3 W m^{-1} K^{-1}, 2.0 W m^{-1} K^{-1} and 0.05 cm^3 cm^{-3}, respectively.

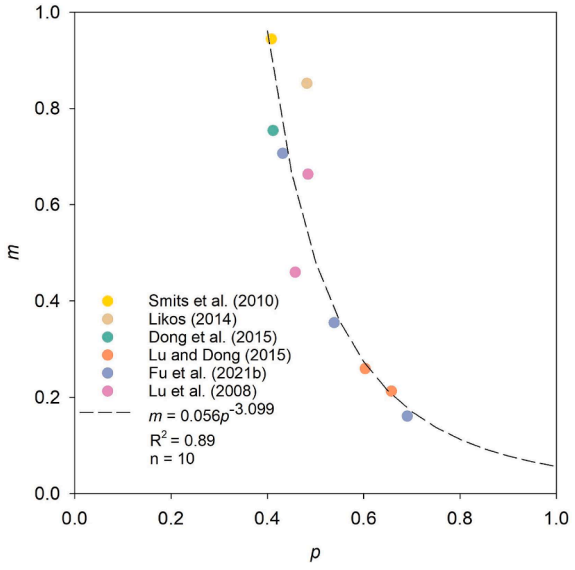

Fig. 3. The relationship between vG model parameter m values and LD model parameter p values for Soils 1–10. The dashed curve is the least squares regression fit of the $m(p)$ equation (Eq. (10)).

Table 4
Fitted parameters of LD model (Eqs. (2)–(4)) and vG model (Eq. (1)) for Soils 1–10 in this study. All the parameters for Soils 1–5 are from Table 1 and Fig. 6a of Lu and Dong (2015).

	LD model				vG model			
	λ_{sat}	λ_{dry}	θ_f	p	θ_s	θ_r	α	m
Soil No.	W m^{-1} K^{-1}	W m^{-1} K^{-1}	cm^3 cm^{-3}		cm^3 m^{-3}	cm^3 m^{-3}	m^{-1}	
1	2.910	0.287	0.008	0.41	–	0.028	5.80	0.94
2	2.500	0.230	0.032	0.48	–	0.010	1.50	0.85
3	3.100	0.290	0.012	0.41	–	0.020	7.70	0.75
4	1.157	0.432	0.130	0.60	–	0.065	0.71	0.26
5	1.556	0.239	0.087	0.66	–	0.050	0.61	0.21
6	2.985	0.303	0.033	0.43	0.368	0.008	3.66	0.71
7	1.223	0.172	0.109	0.54	0.567	0.016	1.18	0.35
8	1.368	0.204	0.231	0.69	0.560	0.094	1.19	0.16
9	1.803	0.244	0.055	0.46	0.428	0.061	3.00	0.46
10	1.582	0.225	0.069	0.48	0.465	0.068	0.71	0.66

clay content ranging from 0 to 100) and bulk density (ranging from 1.05 to 1.77 g cm^{-3}). Fig. 3 shows the m values of the 10 soils (Soils 1–10) as a function of p. Because m decreased nonlinearly with increasing p, a power function equation was used to describe the relationship. The following empirical relationship between m and p was developed for $0.4 < p < 0.7$,

$$m = 0.056p^{-3.099} \quad (10)$$

Thus, an empirical method to estimate θ(ψ) curves from measured λ(θ) data and other soil property values (i.e., soil bulk density, texture, particle density and organic carbon content) is established, and it is hereafter denoted as the "thermal conductivity-water retention (TCWR)" approach (Eqs. (5), (6), (7) and (10)). Here we briefly explain the three key steps of the TCWR approach:

Step 1: λ_{sat}, λ_{dry} θ_s and α are estimated from soil organic carbon content, bulk density, particle density and soil texture using Eqs. (3)–(5) and (7).

Step 2: Fit Eq. (2) to measured λ(θ) values while using the estimated λ_{sat} and λ_{dry} values from Step 1, to determine the remaining LD model fitting parameters, θ_f and p.

Step 3: Estimate the θ_r value from Eq. (6) and calculate the m values from Eq. (10).

4.4. Validation of the TCWR approach

We evaluated the performance of the new TCWR approach with measurements from Soils 11–16. As shown in Fig. 4, most of the estimated θ(ψ) curves for the TCWR method followed the patterns of the measured θ(ψ) curves, which indicated that the TCWR method accurately estimated the θ(ψ) curves. An exception was observed for Soil 16: The θ(ψ) curve estimated with the TCWR approach was flatter and gave larger θ estimates for the larger |ψ| values. These deviations implied an underestimation of parameter m with Eq. (10), because the slope (dθ/d|ψ|) of the θ(ψ) curve was determined mainly by parameter m (van Genuchten et al., 1980). Despite the errors with Soil 16, the TCWR approach generally provided reliable θ(ψ) estimates on the other five soils.

Fig. 5 presents the θ values estimated with the TCWR model at the selected ψ values versus the measured θ data. In general, the estimated θ

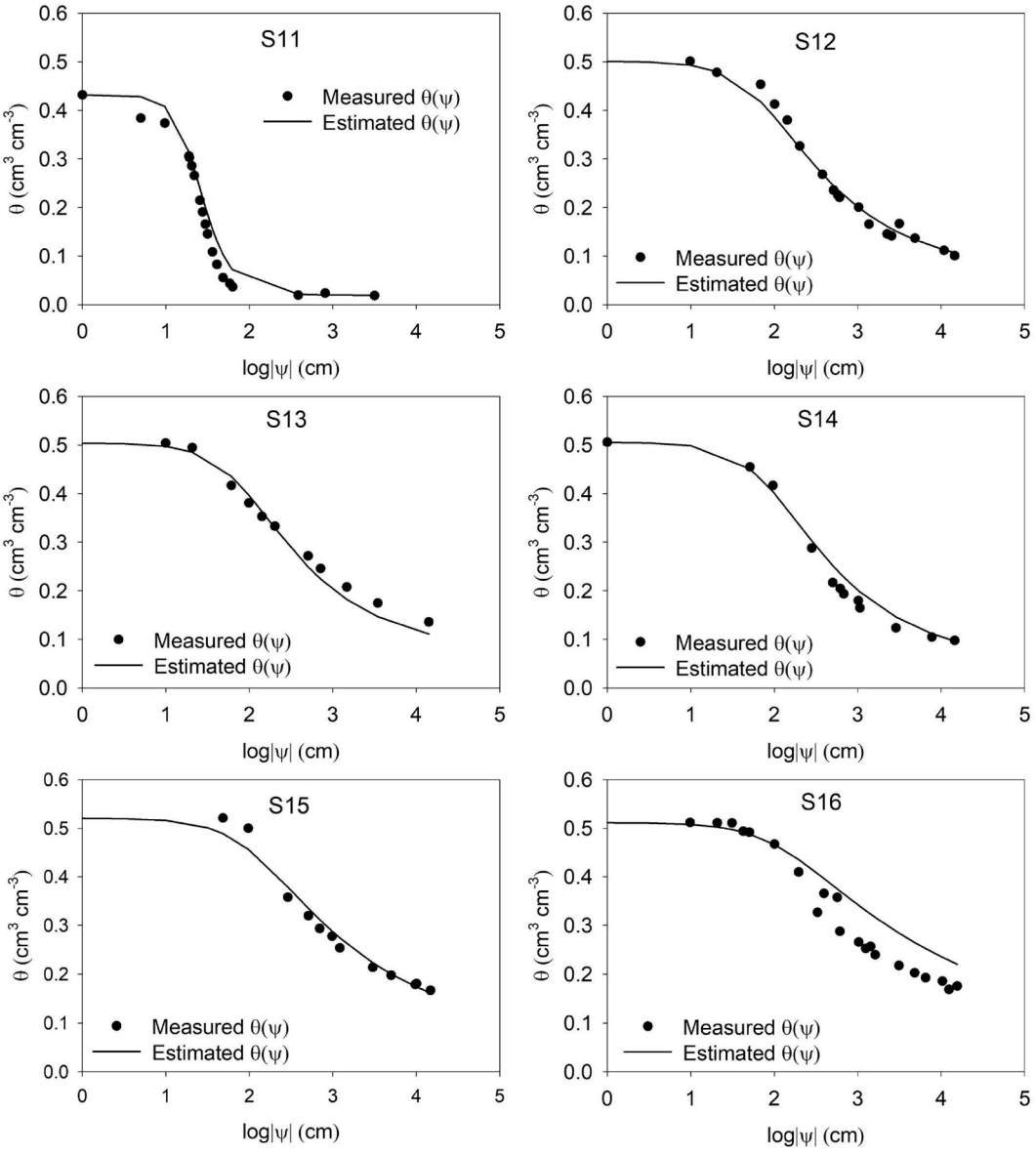

Fig. 4. Measured and estimated soil water retention curves (θ(ψ)) for Soils 11–16, where the circles indicate measured values, and the solid curves indicate θ(ψ) curves estimated by the thermal conductivity-water retention, TCWR, method (Eqs. (5), (6), (7) and (10)).

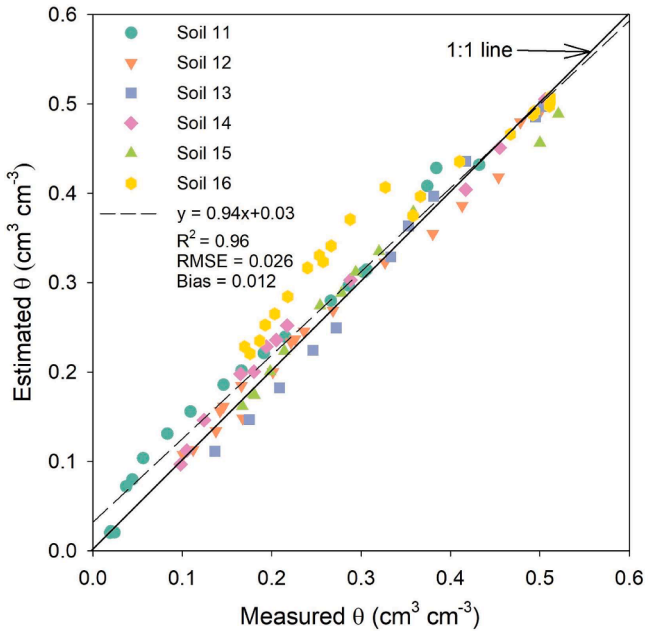

Fig. 5. Comparison of estimated soil θ by the thermal conductivity-water retention, TCWR, approach (Eqs. (5), (6), (7) and (10)) with measured θ at the same soil matric potential values, ψ, for Soils 11–16 in this study. The dashed line indicates the fitted linear regression for the estimated and measured θ values.

Table 5
The root mean square error (RMSE), bias and coefficient of determination (R^2) between measured water content values and thermal conductivity-water retention, TCWR, (Eqs. (5), (6), (7) and (10)) estimated water content values for Soils 11–16 in this study.

Soil no.	Texture	RMSE	Bias	R^2
		$cm^3\ cm^{-3}$	$cm^3\ cm^{-3}$	
11	sand	0.030	0.024	0.98
12	silt loam	0.015	−0.002	0.99
13	silty clay loam	0.019	−0.009	0.99
14	silt loam	0.022	0.015	0.99
15	silty clay loam	0.020	0.001	0.98
16	silt loam	0.052	0.040	0.97
Average		**0.026**	**0.012**	**0.96**

values compared well to the measured θ values. For all of the soils, the coefficients of determination (R^2) were greater than 0.97, which indicated that the TCWR approach provided reliable estimates. The RMSE and bias of the estimated values ranged from 0.015 to 0.052 $cm^3\ cm^{-3}$ and from −0.009 to 0.040 $cm^3\ cm^{-3}$, and the average RMSE and bias of estimated values were 0.026 $cm^3\ m^{-3}$ and 0.012 $cm^3\ cm^{-3}$, respectively (Table 5). Thus, the TCWR approach provided accurate θ(ψ) estimates.

4.5. Further applications

The TCWR approach requires measured λ(θ) data and four soil property values (i.e., organic carbon content, bulk density, particle density and texture) as inputs. For a specific soil, soil particle density and texture are relatively constant in time and organic carbon content changes slowly (thus it can be assumed as constant in the short term), and all are generally available from soil survey. Thus, only the dynamic information for λ, θ, and ρ_b are required to estimate dynamic θ(ψ) curves. Previous studies have shown that by using the thermo-TDR technique, it is possible to measure spatial and temporal variations of λ, θ, and ρ_b (Liu et al., 2014; Zhang et al., 2017; Tian et al., 2018; Fu et al., 2019, 2020, 2021a). Thus, the TCWR approach has the potential to estimate dynamic θ(ψ) curves with time and depth under field conditions.

Electrical conductivity (σ) depends on the same soil properties (e.g., θ, ρ_b and particle size distribution) as λ does (Abu-Hamdeh and Reeder 2000; Friedman 2005). Based on the similarity between electrical current and water flow, Fu et al. (2021b) presented a model to estimate a θ(ψ) curve from bulk electrical conductivity (σ)-water content measurements. Although σ data are more readily available than λ measurements (because of the widespread use of TDR sensors for monitoring θ and σ), the new TCWR approach developed in this study has some advantages. First, λ has less temperature dependence than does σ at ambient soil temperatures (Nouveau et al., 2016). This is especially crucial in field conditions where soil temperature shows obvious spatial and temporal variations. Second, both models require inputs (λ or σ) at dry and saturated conditions. As mentioned above, both λ_{sat} and λ_{dry} are functions of ρ_b, which can be estimated indirectly. In contrast, no universal equation is available to estimate indirectly the σ values at dry and saturated conditions, which limits certain field applications of the electrical conductivity-based approach.

5. Conclusion

A TCWR approach was developed to estimate the parameters of the van Genuchten θ(ψ) model from λ(θ) measurements and soil properties (organic carbon content, bulk density, particle density and soil texture). The new approach was calibrated with data collected on 10 soils representing a wide range of textures, and was evaluated with θ(ψ) data from six additional soils. Overall, the TCWR method performed well. The new method has a potential to estimate dynamic field θ(ψ) curves continuously from dynamic λ(θ) measurements.

CRediT authorship contribution statement

Yongwei Fu: Conceptualization, Methodology, Formal analysis, Writing – original draft. **Sen Lu:** Resources, Writing – review & editing. **Tusheng Ren:** Resources, Writing – review & editing. **Robert Horton:** Conceptualization, Writing – review & editing. **J.L. Heitman:** Supervision, Conceptualization, Writing – review & editing.

Declaration of Competing Interest

The authors declare that they have no known competing financial interests or personal relationships that could have appeared to influence the work reported in this paper.

Acknowledgements

This research was supported by the China Scholarship Council, US Army Research Laboratory (Grant Number: W911NF-16-1-0287), US National Science Foundation (Grant Number: 2037504), USDA-NIFA Multi-State Project 4188 and Natural Science Foundation of China (Grant Number: 41877019).

References

Abu-Hamdeh, N.H., Reeder, R.C., 2000. Soil thermal conductivity effects of density, moisture, salt concentration, and organic matter. Soil Sci. Soc. Am. J. 64 (4), 1285–1290.
Bescansa, P., Imaz, M.J., Virto, I., Enrique, A., Hoogmoed, W.B., 2006. Soil water retention as affected by tillage and residue management in semiarid Spain. Soil Tillage Res. 87 (1), 19–27.
Brooks, R.H., Corey, A.T., 1964. Hydraulic properties of porous medium. Colorado State University, USA.
Campbell, G.S., 1974. A simple method for determining unsaturated conductivity from moisture retention data. Soil Sci. 117 (6), 311–314.
Côté, J., Konrad, J.-M., 2009. Assessment of structure effects on the thermal conductivity of two-phase porous geomaterials. Int. J. Heat Mass Tran 52 (3-4), 796–804.

Dane, J.H., Hopmans, J.W., 2002. Water retention and storage. In: Dane, J.H., Topp, G.C. (Eds.), Methods of Soil Analysis. Part. 4. Physical Methods. SSSA, Madison, WI, pp. 671–796.
Dexter, A.R., Czyż, E.A., Richard, G., Reszkowska, A., 2008. A user-friendly water retention function that takes account of the textural and structural pore spaces in soil. Geoderma 143 (3-4), 243–253.
Dong, Y.i., McCartney, J.S., Lu, N., 2015. Critical review of thermal conductivity models for Unsaturated Soils. Geotech. Geol. Eng. 33 (2), 207–221.
Ewing, R.P., Horton, R., 2007. Thermal conductivity of a cubic lattice of spheres with capillary bridges. J. Phys. D Appl. Phys. 40 (16), 4959–4965.
Fredlund, D.G., Xing, A., 1994. Equations for the soil–water characteristic curve. Can. Geotech. J. 31 (4), 521–532.
Friedman, S.P., 2005. Soil properties influencing apparent electrical conductivity: a review. Comput Electron Agr 46 (1-3), 45–70.
Fu, Y., Tian, Z., Amoozegar, A., Heitman, J., 2019. Measuring dynamic changes of soil porosity during compaction. Soil Tillage Res. 193, 114–121.
Fu, Y., Lu, Y., Heitman, J., Ren, T., 2020. Root-induced changes in soil thermal and dielectric properties should not be ignored. Geoderma 370, 114352. https://doi.org/10.1016/j.geoderma.2020.114352.
Fu, Y., Lu, Y., Heitman, J., Ren, T., 2021a. Root influences on soil bulk density measurements with thermo-time domain reflectometry. Geoderma 403, 115195.
Fu, Y., Horton, R., Heitman, J., 2021b. Estimation of soil water retention curves from soil bulk electrical conductivity and water content measurements. Soil Tillage Res. 209, 104948. https://doi.org/10.1016/j.still.2021.104948.
He, H., Dyck, M., Lv, J., 2020. A new model for predicting soil thermal conductivity from matric potential. J. Hydol. 589, 125167. https://doi.org/10.1016/j.jhydrol.2020.125167.
Howard, P.J.A., Howard, D.M., 1990. Use of organic carbon and loss-on-ignition to estimate soil organic matter in different soil types and horizons. Biol. Fertil. Soils 9 (4), 306–310.
Johansen, O., 1975. Thermal conductivity of soils. Ph.D. diss. Norwegian Univ. of Science and Technol., Trondheim (CRREL draft transl. 637, 1977).
Kim, D., Kim, G., Baek, H., 2015. Relationship between thermal conductivity and soil–water characteristic curve of pure bentonite-based grout. Int. J. Heat Mass Tran. 84, 1049–1055.
Kosugi, K., 1994. Three-parameter lognormal distribution model for soil water retention. Water Resour. Res. 30 (4), 891–901.
Likos, W.J., 2014. Modeling thermal conductivity dryout curves from soil-water characteristic curves. J. Geotech. Geoenviron. Eng. 140 (5), 04013056. https://doi.org/10.1061/(ASCE)GT.1943-5606.0001078.
Lipiec, J., Usowicz, B., Ferrero, A., 2007. Impact of soil compaction and wetness on thermal properties of sloping vineyard soil. Int. J. Heat. Mass Tran. 50 (19-20), 3837–3847.
Liu, X., Lu, S., Horton, R., Ren, T., 2014. In situ monitoring of soil bulk density with a thermo-TDR sensor. Soil Sci. Soc. Am. J. 78 (2), 400–407.
Lu, N., Likos, J.W., 2004. Unsaturated soil mechanics. Wiley, Hoboken, NJ.
Lu, N., Dong, Y., 2015. Closed-form equation for thermal conductivity of unsaturated soils at room temperature. J. Geotech. Geoenviron. Eng. 141 (6), 04015016. https://doi.org/10.1061/(ASCE)GT.1943-5606.0001295.
Lu, S., Ren, T., Gong, Y., Horton, R., 2007. An improved model for predicting soil thermal conductivity from water content at room temperature. Soil Sci. Soc. Am. J. 71 (1), 8–14.
Lu, S., Ren, T., Gong, Y., Horton, R., 2008. Evaluation of three models that describe soil water retention curves from saturation to oven dryness. Soil Sci. Soc. Am. J. 72 (6), 1542–1546.
Lu, S., Lu, Y., Peng, W., Ju, Z., Ren, T., 2019. A generalized relationship between thermal conductivity and matric suction of soils. Geoderma 337, 491–497.
Lu, Y., Liu, X., Zhang, M., Heitman, J.L., Horton, R., Ren, T., 2017. Thermo-time domain reflectometry method: Advances in monitoring in situ soil bulk density. Method. Soil Anal. 2.
McCumber, M.C., Pielke, R.A., 1981. Simulation of the effects of surface fluxes of heat and moisture in a mesoscale numerical model. J. Geophys. Res. 86, 9929–9938.
Merdun, H., Çınar, Ö., Meral, R., Apan, M., 2006. Comparison of artificial neural network and regression pedotransfer functions for prediction of soil water retention and saturated hydraulic conductivity. Soil Tillage Res. 90 (1-2), 108–116.
Mitarai, N., Nori, F., 2006. Wet granular materials. Adv. Phys. 55 (1-2), 1–45.
Miyata, S., Kosugi, K., Gomi, T., Onda, Y., Mizuyama, T., 2007. Surface runoff as affected by soil water repellency in a Japanese cypress forest. Hydrol. Process. 21 (17), 2365–2376.
Nouveau, M., Grandjean, G., Leroy, P., Philippe, M., Hedri, E., Boukcim, H., 2016. Electrical and thermal behavior of unsaturated soils: Experimental results. J. Appl. Geophys. 128, 115–122.
Ochsner, T.E., Baker, J.M., 2008. In situ monitoring of soil thermal properties and heat flux during freezing and thawing. Soil Sci. Soc. Am. J. 72 (4), 1025–1032.
Omuto, C.T., 2009. Biexponential model for water retention characteristics. Geoderma 149 (3-4), 235–242.
Rawls, W.J., Brakensiek, D.L., 1985. Prediction of soil water properties for hydrologic modeling. In: Jones, E.B., Ward, T.J. (Eds.), Watershed Management in the Eighties. American Society of Civil Engineers, Reston, Virginia, pp. 293–299.
Reece, C.F., 1996. Evaluation of a line heat dissipation sensor for measuring soil matric potential. Soil Sci. Soc. Am. J. 60 (4), 1022–1028.
Ren, T., Noborio, K., Horton, R., 1999. Measuring soil water content, electrical conductivity, and thermal properties with a thermo-time domain reflectometry probe. Soil Sci. Soc. Am. J. 63 (3), 450–457.
Revil, A., Lu, N., 2013. Unified water isotherms for clayey porous materials. Water Resour. Res. 49 (9), 5685–5699.
Schaap, M.G., Bouten, W., 1996. Modeling water retention on curves of sandy soils using neural networks. Water Resour. Res. 32, 3033–3040.
Schaap, M.G., Leij, F.J., 1998. Using neural networks to predict soil water retention and soil hydraulic conductivity. Soil Tillage Res. 47, 37–42.
Smits, K.M., Sakaki, T., Limsuwat, A., Illangasekare, T.H., 2010. Thermal conductivity of sands under varying moisture and porosity in drainage–wetting Cycles. Vadose Zo. J. 9 (1), 172–180.
Tarnawski, V.R., Leong, W.H., 2000. Thermal conductivity of soils at very low moisture content and moderate temperatures. Transp. Porous Media 41, 137–147.
Tarnawski, V.R., Gori, F., 2002. Enhancement of the cubic cell soil thermal conductivity model. Int. J. Energy Res. 26 (2), 143–157.
Tian, Z., Lu, Y., Ren, T., Horton, R., Heitman, J.L., 2018. Improved thermo-time domain reflectometry method for continuous in-situ determination of soil bulk density. Soil Tillage Res. 178, 118–129.
Tuller, M., Or, D., Dudley, L.M., 1999. Adsorption and capillary condensation in porous media: Liquid retention and interfacial configurations in angular pores. Water Resour. Res. 35 (7), 1949–1964.
van Genuchten, M.T., 1980. A closed-form equation for predicting the hydraulic conductivity of unsaturated soils. Soil Sci. Soc. Am. J. 44 (5), 892–898.
Vereecken, H., Maes, J., Feyen, J., Darius, P., 1989. Estimating the soil-moisture retention characteristic from texture, bulk density, and carbon content. Soil Sci. 148 (6), 389–403.
Vereecken, H., Weynants, M., Javaux, M., Pachepsky, Y., Schaap, M.G., van Genuchten, M.T., 2010. Using pedotransfer functions to estimate the van Genuchten-Mualem soil hydraulic properties: a review. Vadose Zone J. 9 (4), 795–820.
Wayllace, A., Lu, N., 2012. A transient water release and imbibitions method for rapidly measuring wetting and drying soil water retention and hydraulic conductivity functions. Geotech. Test. J. 35 (1), 103596. https://doi.org/10.1520/GTJ103596.
Weynants, M., Vereecken, H., Javaux, M., 2009. Revisiting Vereecken pedotransfer functions: introducing a closed-form hydraulic model. Vadose Zo. J. 8 (1), 86–95.
Wösten, J.H.M., Pachepsky, Y.A., Rawls, W.J., 2001. Pedotransfer functions: bridging the gap between available basic soil data and missing soil hydraulic characteristics. J. Hydrol. 251 (3-4), 123–150.
Zhang, M., Lu, Y., Heitman, J., Horton, R., Ren, T., 2017. Temporal changes of soil water retention behavior as affected by wetting and drying following tillage. Soil Sci. Soc. Am. J. 81 (6), 1288–1295.